dosage is important because an increase in the dose limits the adjuvant effect (*18*). The amounts of NAGO that produced optimal adjuvant effects (~5 μg of GO, <50 ng of NA) are likely to be substantially less than natural exposure to ubiquitous microbial enzymes. Antibodies reacting with NA and GO were detectable in normal mouse serum. Anti-NA titers were unchanged after single NAGO use, whereas anti-GO titers were increased fivefold.

Because galactose oxidation does not compete in the conventional adjuvant pathways, it might be used in combination with conventional adjuvants and vehicles. It was not compatible with alum but showed good synergy with muramyl dipeptide (*19*) in mice (*20*). On its own, galactose oxidation was particularly potent in inducing T_H cell priming and T cell cytotoxicity and seems well suited to prophylactic applications where such responses are important (*15, 21–28*). Such use depends, of course, on the sustained absence of adverse reactions, and in this respect the absence of adverse reactions in mice looks promising.

REFERENCES AND NOTES

1. A. T. Glenny, G. C. G. Pope, H. Waddington, U. Wallace, *Chem. Ind.*, p. 415 (15 June 1926).
2. G. Gregoriadis, A. C. Allison, G. Poste, Eds., *Immunological Adjuvants and Vaccines* (Plenum, New York, 1989); M. K. Hart *et al.*, *J. Immunol.* **145**, 2677 (1990).
3. C. K. Stover *et al.*, *Nature* **351**, 456 (1991).
4. R. H. Schwartz, *Annu. Rev. Immunol.* **3**, 237 (1985); S. Buus, A. Sette, H. M. Grey, *Immunol. Rev.* **98**, 115 (1987).
5. T. A. Springer, *Nature* **345**, 426 (1990).
6. J. Rhodes, *J. Immunol.* **143**, 1482 (1989); X.-M. Gao and J. Rhodes, *ibid.* **144**, 2883 (1990); J. Rhodes, *ibid.* **145**, 463 (1990).
7. A. Novogrodsky and E. Katchalski, *Proc. Natl. Acad. Sci. U.S.A.* **70**, 1824 (1973).
8. Neuraminidase (E.C. 3.2.1.18) was from *Vibrio cholerae* (25 U per microgram of protein, BDH Poole, Dorset, United Kingdom). Galactose oxidase (E.C. 1.1.3.9) was from *Dactylium dendroides* (800 U per milligram of protein, Sigma). Standard adjuvant doses were as follows: NAGO: 1 U of NA plus 5 U of GO in 100 μl of phosphate-buffered saline (PBS) containing Ag (mixed immediately before injection); FCA (Difco): 50 μl of Ag solution emulsified in 50 μl of FCA; saponin (Quil A, Superfos, Denmark): 50 μg in 100 μl of PBS containing Ag; alum (Wellcome, Beckenham, United Kingdom): 100 μg in 100 μl of PBS containing Ag. Heat inactivation of NAGO completely abrogated the adjuvant effect. Excess D-galactose was inhibitory. GO responses were 50 to 70% of NAGO responses.
9. L. A. Lasky *et al.*, *Science* **233**, 209 (1986).
10. B. Zheng and J. Rhodes, unpublished data.
11. X.-M. Gao, F. Y. Liew, J. P. Tite, *J. Immunol.* **143**, 3007 (1989).
12. I. G. Charles *et al.*, *Proc. Natl. Acad. Sci. U.S.A.* **86**, 3554 (1989).
13. V. F. Murphy, W. C. Rowan, M. J. Page, A. A. Holder, *Parasitology* **100**, 177 (1990).
14. M. R. Lifely *et al.*, *Vaccine* **9**, 60 (1991).
15. X.-M. Gao, B. Zheng, F. Y. Liew, S. J. Brett, J. P. Tite, *J. Immunol.* **147**, 3268 (1991).
16. P. M. Taylor, J. Davey, K. Howland, J. Rothbard, B. A. Askonas, *Immunogenetics* **26**, 267 (1987).
17. B. Zheng, S. J. Brett, J. Rhodes, unpublished data.
18. B. Zheng and J. Rhodes, unpublished data.
19. L. Chedid, F. Audibert, P. Lefrancier, J. Choay, E. Lederer, *Proc. Natl. Acad. Sci. U.S.A.* **73**, 2472 (1976).
20. B. Zheng and J. Rhodes, unpublished data.
21. G. L. Ada, *Lancet* **335**, 523 (1990).
22. Y.-L. Lin and B. A. Askonas, *J. Exp. Med.* **154**, 225 (1981).
23. K.-L. Yap, G. L. Ada, I. F. C. McKenzie, *Nature* **273**, 238 (1978).
24. R. M. Ruprecht *et al.*, *Proc. Natl. Acad. Sci. U.S.A.* **87**, 5558 (1990).
25. J. H. L. Playfair, J. M. Blackwell, H. R. P. Miller, *Lancet* **335**, 1263 (1990).
26. G. C. Schild and P. D. Minor, *ibid.*, p. 1081 (1990).
27. W. C. Koff and A. S. Fauci, *AIDS* **3** (suppl. 1), S125 (1989).
28. K. S. Furukawa, K. Furukawa, F. X. Real, L. J. Old, K. O. Lloyd, *J. Exp. Med.* **169**, 583 (1989).

29. We are grateful to R. Bomford for HIV gp120. We thank M. Lockyear for PMMSA and M. Roberts for P69. We thank B. Pearce and J. Esdaile for technical assistance, and M. Stapleton for performing an enzyme-linked immunosorbent assay (ELISA) capture assay.

15 November 1991; accepted 24 March 1992

Calcium Entry Through Kainate Receptors and Resulting Potassium-Channel Blockade in Bergmann Glial Cells

T. Müller, T. Möller, T. Berger,* J. Schnitzer,† H. Kettenmann‡

Glutamate receptors, the most abundant excitatory transmitter receptors in the brain, are not restricted to neurons; they have also been detected on glial cells. Bergmann glial cells in mouse cerebellar slices revealed a kainate-type glutamate receptor with a sigmoid current-to-voltage relation, as demonstrated with the patch-clamp technique. Calcium was imaged with fura-2, and a kainate-induced increase in intracellular calcium concentration was observed, which was blocked by the non–*N*-methyl-D-aspartate (NMDA) glutamate receptor antagonist 6-cyano-7-nitroquinoxaline-2,3-dione (CNQX) and by low concentrations of external calcium, indicating that there was an influx of calcium through the kainate receptor itself. The entry of calcium led to a marked reduction in the resting (passive) potassium conductance of the cell. Purkinje cells, which have glutamatergic synapses, are closely associated with Bergmann glial cells and therefore may provide a functionally important stimulus.

During the development of the cerebellum, Bergmann glial cells provide the guiding structures for the migrating granule cells (*1*). In contrast, little is known about their function in the adult animal despite the fact that their complex architecture and intimate contacts with the Purkinje cells suggest an interaction between these two cell types. Recent studies have challenged the view of the glial cells as electrically passive elements in the brain by demonstrating the presence of many transmitter receptors, including those for glutamate (*2*). In situ hybridization studies indicate the expression of kainate-binding proteins on Bergmann glial cells (*3*). Although the subunits of the α-amino-3-hydroxy-5-methyl-4-isoxazolepropionate (AMPA)–kainate receptor channel GluR-A and GluR-D are expressed in these cells, the ubiquitous GluR-B subunit was not found (*4*). Recombinant GluR-A and GluR-D receptors exhibit a behavior distinct from other kainate receptors; namely, they have a doubly rectifying current-voltage (*I-V*) relation and high Ca^{2+} permeability (*4*).

We have used isolated slices of the mouse cerebellum to analyze membrane properties of Bergmann glial cells in situ with the patch-clamp technique (*5*) and with a fura-2–based Ca^{2+} imaging system (*6*). The Bergmann glial cell somata were recognized by their location in the Purkinje cell layer and by their small diameter (5 to 10 μm). Filling the cells with the fluorescent dyes Lucifer yellow (*7*) or fura-2 revealed the typical morphology of Bergmann glial cells: two to six processes extended through the molecular layer and terminated at the pia with the formation of glial end feet (Fig. 1, A and B). Eleven of the cells injected with Lucifer yellow were positively stained for glial fibrillary acidic protein, identifying them as astrocyte-like cells (Fig. 1C) (*8*).

Patch-clamp recordings demonstrated that the membrane was characterized by a large K^+ conductance with no sign of voltage- or time-dependent gating (Fig. 1D). Currents were observed with depolarizing and hyperpolarizing voltage steps, and the

T. Müller, T. Möller, T. Berger, H. Kettenmann, Department of Neurobiology, University of Heidelberg, Im Neuenheimer Feld 345, W-6900 Heidelberg, Germany.
J. Schnitzer, Max Planck Institute for Brain Research, Deutschordenstrasse 46, W-6000 Frankfurt, Germany.

*Present address: Institute for Anatomy, Albertstrasse 17, W-7800 Freiburg, Germany.
†Present address: Center for Molecular Medicine, Robert-Rössle-Strasse 10, O-1115 Berlin-Buch, Germany.
‡To whom correspondence should be addressed.

I-V relation was linear (Fig. 1F). As expected for a K^+-selective conductance, the reversal potential of these currents followed the K^+ gradient; when the extracellular K^+ concentration was increased from 5 to 25 mM, the reversal potential shifted from −80 to −40 mV. The membrane potential measured after establishing the whole-cell recording configuration was between −60 and −70 mV (n = 50) and thus was close to the K^+ equilibrium potential. Although the K^+-channel blockers Ba^{2+} (10 mM in the bathing solution), Cs^+ (130 mM in the pipette solution), and apamin (10^{-9} M in the bathing solution) were not effective or were only slightly effective in reducing these passive currents, they were markedly blocked when cytosolic Ca^{2+} was increased by adding the Ca^{2+} ionophore ionomycin (Figs. 1E, 2B, and 3A). The effectiveness of ionomycin varied among cells. In some cells 80% of the current was blocked after 3 min; in others a 50% blockade was observed after 30 min.

Glutamate (n = 5; 10^{-3} M; range, 20 to 174 pA) and kainate (n = 50; 10^{-3} M; range, 71 to 1574 pA) induced an inward current in Bergmann glial cells. We determined the reversal potential of the kainate-induced current while the resting K^+ conductance was blocked by exposing the slice for 30 min to ionomycin. The membrane was clamped from a resting value of −70 mV to −40, −20, 0, 20, 40, 60, 100, and −105 mV for 100-ms durations separated by 100-ms intervals. This clamp protocol was repetitively used (every 2 s) before, during, and after addition of kainate (Fig. 2). The kainate-induced currents were obtained by subtracting currents at a specific membrane potential in the presence of kainate from those recorded before the application of kainate. The resulting *I-V* relation was sigmoidal; that is, it was outwardly rectifying at positive potentials and inwardly rectifying at negative potentials (Fig. 2C), similar to that described for the recombinant GluR-A–GluR-D receptor (*4*). The kainate-induced currents reversed

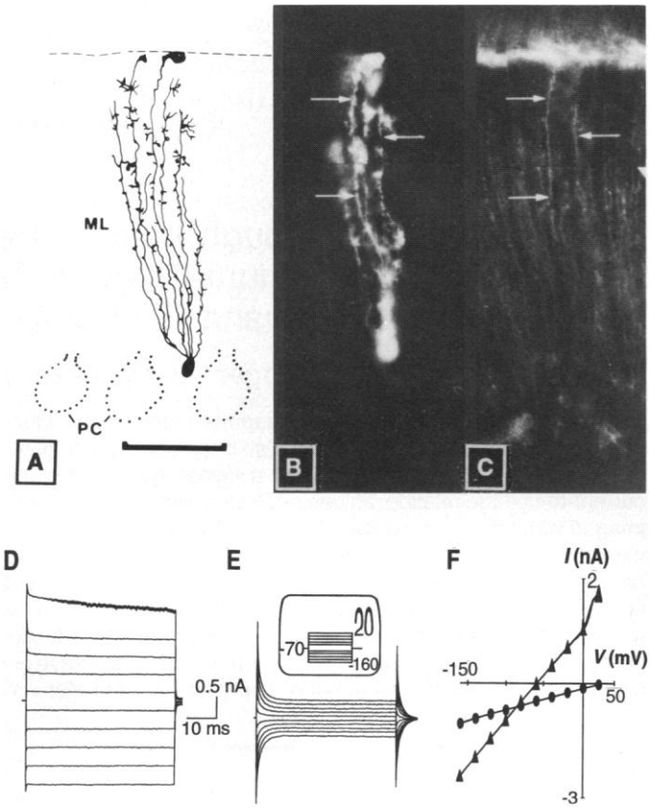

Fig. 1. Identification of recorded Bergmann glial cells. A Bergmann glial cell was filled with the fluorescent dye Lucifer Yellow by dialysis of the cell with the pipette solution after the establishment of a whole-cell patch-clamp recording. (**A**) The camera lucida drawing and (**B**) the fluorescent photomicrograph illustrate the extension of the cell in the molecular (ML) and Purkinje cell layer (PC) in a cerebellar slice from a 20-day-old mouse. Three of the four processes form end feet at the pial surface. Bar, 100 μm. (**C**) A double immunofluorescence of the same slice illustrates the distribution of glial fibrillary acidic protein (GFAP), a marker for astrocytes and Bergmann glial cells. The arrows in (B) and (C) point to corresponding Lucifer Yellow–filled and GFAP-positive processes. (**D**) Membrane currents were recorded from a Bergmann glial cell activated by depolarizing and hyperpolarizing potentials ranging from −160 to 20 mV, with 20-mV increments [inset in (E)]. Currents showed no time-dependent activation or inactivation. (**E**) Thirty minutes after exposure to ionomycin (10 μM, 15 s), currents were recorded from the same cell and with a similar protocol as in (D). (**F**) An *I-V* curve was constructed from recordings in (D) (▲) and (E) (●). The reversal potential shifted from −56 to 26 mV after application of ionomycin.

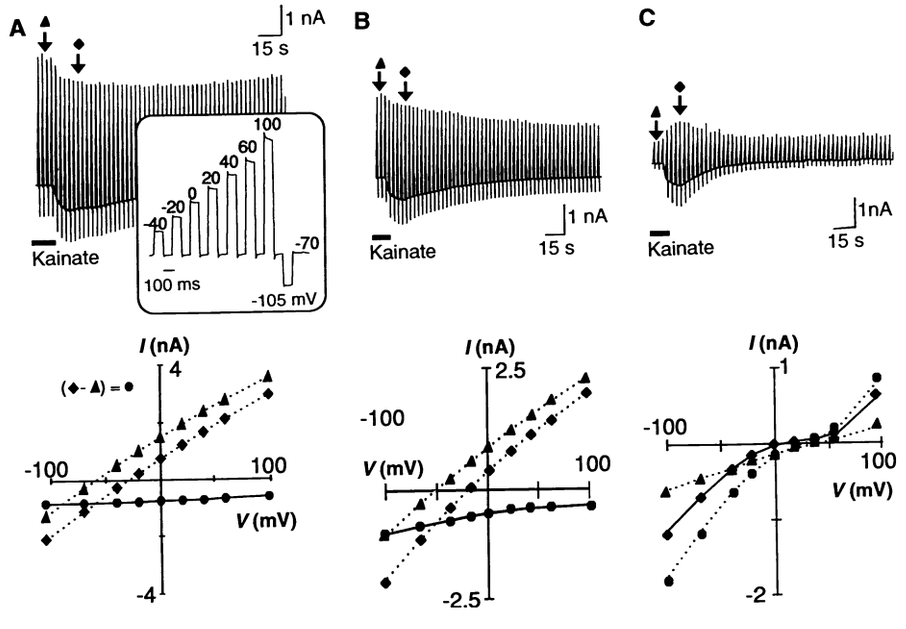

Fig. 2. Effect of kainate on membrane currents. (**A**) Membrane currents were recorded from a Bergmann glial cell before, during, and after application of kainate (10^{-3} M). Holding potential, −70 mV. With a voltage-clamp protocol, the membrane was depolarized or hyperpolarized for 100-ms intervals to −40, −20, 0, 20, 40, 60, 100, and −105 mV (inset). With this voltage-clamp protocol, *I-V* curves were constructed at 2-s intervals. Three *I-V* curves were averaged before (▲) and at the peak of the kainate response (◆) and are displayed at the bottom. The kainate-induced current was obtained by subtracting the current before from that at the peak of the kainate response (●). There is no apparent kainate-induced conductance increase. (**B**) A recording protocol similar to that in (A) was obtained from the same cell 5 min after application of the Ca^{2+} ionophore ionomycin (10 μM, 15 s). (**C**) Current and *I-V* curve 40 min after application of ionomycin. The membrane conductance was 18% of its original value.

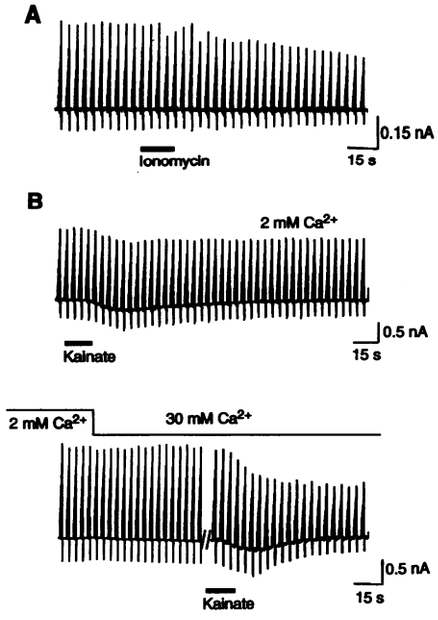

Fig. 3. (**A**) Effect of ionomycin on resting currents. Membrane currents were recorded as described in Fig. 2 while the membrane was clamped to depolarizing and hyperpolarizing values from a resting value of −70 mV. Ionomycin (10 μM, 15 s) was applied (bar). (**B**) Kainate-induced currents in different extracellular Ca^{2+} concentrations. With a similar recording protocol as in (A), kainate (10^{-3} M) was applied in bathing solution containing normal extracellular Ca^{2+} (2 mM, upper trace). Extracellular Ca^{2+} was then increased to 30 mM (lower trace). The recording was interrupted for 5 min as indicated by the parallel bars.

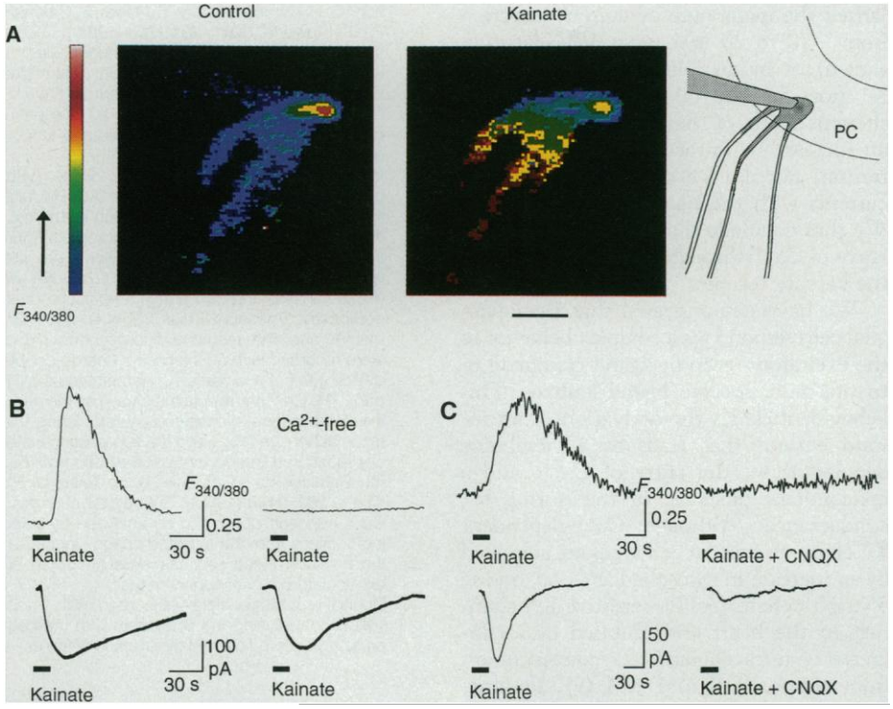

Fig. 4. (**A**) Kainate-induced changes in intracellular Ca^{2+}. A Bergmann glial cell was filled with fura-2 by dialysis with the patch pipette solution. The bar on the left indicates the change in the fluorescence ratio ($F_{340/380}$) (colors on the bottom indicate low Ca^{2+} concentrations). The diagram on the right outlines the extension of the Bergmann glial cell with the pipette still attached on the soma. Three processes can be distinguished. Bar, 20 μm. The color-coded pictures illustrate the increase in Ca^{2+} concentration during application of kainate (1 mM, middle) as compared to the control before (left). In the presence of kainate, the tips of the processes disappear because of saturation of the Ca^{2+} imaging system. (**B**) Effect of low extracellular Ca^{2+} concentration. From a series of Ca^{2+} images as described in (A), continuous traces of changes in intracellular Ca^{2+} concentration were constructed by averaging the changes in the cell processes. (Top) Application of kainate leads to an increase in the fluorescence ratio, indicative of an increase in Ca^{2+} concentration ($F_{340/380}$) (left trace). In the Ca^{2+}-free bathing solution, the kainate-induced change in Ca^{2+} concentration is blocked (right trace). (Bottom) The current recordings were obtained simultaneously with the patch-clamp technique. The kainate-induced inward current was not blocked in the Ca^{2+}-free bathing solution. (**C**) Effect of CNQX. As described in (B), the effect of the kainate receptor antagonist CNQX (45 μM) was analyzed. The current and intracellular Ca^{2+} concentration recordings were obtained from two different cells.

at 0 mV (Fig. 2C) (n = 5; range, −15 to 5 mV).

A different type of result was obtained when the resting K^+ current was present: kainate also induced an inward current, but the conductance significantly decreased after application of kainate, and it was not possible to determine a clear reversal potential of the kainate-induced current (Fig. 2A). In some cases the conductance decrease was not fully reversible, and, with repetitive applications of kainate, the membrane conductance decreased in discrete steps to values similar to those observed after a exposure to ionomycin. Under such conditions, a reversal potential of the kainate-induced current could again be determined, which was then close to 0 mV. Figure 2 illustrates the changes in the membrane conductance and kainate-induced currents; in addition, ionomycin was added at a defined time. At −70 mV, kainate always induced an inward current of similar amplitude. However, the voltage jumps to depolarizing potentials revealed a marked reduction of the membrane conductance after the first application of kainate that was only partially reversible. After 40 min of exposure to ionomycin, the resting membrane conductance was decreased to 18% of its initial value and the kainate-induced current reversed at 0 mV. This result can be explained by the entry of Ca^{2+} via the Ca^{2+} ionophore and a resulting blockade of the resting K^+ conductance by the increased intracellular Ca^{2+} concentration. To further strengthen this hypothesis, we increased the extracellular Ca^{2+} concentration from 2 to 30 mM (Fig. 3B). The resting K^+ conductance was not affected by this increase until kainate was applied; then the conductance substantially decreased and did not recover (Fig. 3B) (mean decrease, 42.4%; n = 5). These results suggested that kainate triggers an influx of Ca^{2+}, as described for the recombinant GluR-A–GluR-D receptor (*4*).

To record the changes in intracellular Ca^{2+} concentration, we used a fura-2–based imaging system. Bergmann glial cells were voltage-clamped with the patch-clamp method and filled with fura-2 by dialysis of the cell from the patch pipette. The cells, including their processes, were filled within 10 to 40 min (Fig. 4A). We were thus able to simultaneously record membrane currents and changes in intracellular Ca^{2+} concentration. Application of kainate induced an increase in intracellular Ca^{2+} concentration (n = 10) (Fig. 4A). This increase was reversibly blocked in the Ca^{2+}-free bathing solution, indicating an influx of Ca^{2+} from the extracellular space, whereas the kainate-induced inward current was still observed (n = 3) (Fig. 4B). Application of 45 μM 6-cyano-7-nitroquinoxaline-2,3-dione (CNQX) blocked both the Ca^{2+} entry and the membrane current (n = 5) (Fig. 4C). To exclude participation of voltage-gated Ca^{2+} channels, we depo-

larized the membrane by current injection from −70 to 20 mV (n = 10) (data not shown) or by an increase of extracellular K^+ from 5 to 50 mM (n = 3) (data not shown). None of these experiments led to an increase in intracellular Ca^{2+} concentration, nor did we observe Ca^{2+} inward currents with the patch-clamp technique. We thus conclude that kainate triggers the entry of Ca^{2+} through the intrinsic pore of the kainate receptor channel.

We have demonstrated that Bergmann glial cells respond with complex behavior to the excitatory receptor ligand glutamate or to the more specific ligand kainate. This behavior includes the activation of an inward current that leads to a membrane depolarization, the entry of Ca^{2+}, and a concomitant blockade of the resting K^+ conductance. Although Ca^{2+}-dependent K^+ channels in most cell types are activated by an increase in cytosolic Ca^{2+}, adenosine 5′-triphosphate (ATP)–sensitive K^+ channels in the heart are inhibited by an increase of intracellular Ca^{2+} concentration from nominally 0 to 1 μM (9). Purkinje cells receive glutamatergic input, and the Bergmann glial cells are in intimate contact with these synaptic areas (*10*); excitation of the Purkinje cells may simultaneously trigger a cascade of events in the adjacent Bergmann glial cells. Such events could occur locally but also propagate along the cell. The functional consequences of the glial response are not known. However, the approach of assessing Bergmann glial cells in situ helps to elucidate such neuron-glia interactions.

REFERENCES AND NOTES

1. P. Rakic, *Trends Neurosci.* **4**, 184 (1981); M. E. Hatten, *ibid.* **13**, 179 (1990).
2. G. V. Blankenfeld and H. Kettenmann, *Mol. Neurobiol.* **5**, 31 (1992).
3. P. Gregor, I. Mano, I. Maoz, M. Keown, V. J. Teichberg, *Nature* **342**, 689 (1989).
4. M. Hollmann, M. Hartley, S. Heinemann, *Science* **252**, 851 (1991); H. Monyer, P. H. Seeburg, W. Wisden, *Neuron* **6**, 799 (1991); T. A. Verdoorn, N. Burnashev, H. Monyer, P. H. Seeburg, B. Sakmann, *Science* **252**, 1715 (1991); N. Burnashev *et al.*, *ibid.* **256**, 1566 (1992).
5. Young mice (postnatal day 17 to 22) were killed by decapitation, and 120-μm-thick slices were cut from the cerebellum. Slices were placed on a cover slip under a nylon mesh in a recording chamber [F. Edwards, A. Konnerth, B. Sakmann, T. Takahashi, *Pfluegers Arch.* **414**, 600 (1989)]. Slices were viable under these conditions for more than 3 hours. The chamber was continuously perfused with a salt solution containing 150 mM NaCl, 5.4 mM KCl, 2 mM $CaCl_2$, 1 mM $MgCl_2$, 5 mM Hepes, and 10 mM glucose and gassed with O_2. The pH was adjusted with NaOH to 7.2. Cell somata of the Bergmann glial cells were visible in normal water-immersion optics and could be approached by the patch electrode (pipette resistance ~10 megohms). The pipette contained 130 mM KCl, 0.5 mM $CaCl_2$, 5 mM EGTA, 2 mM $MgCl_2$, 10 mM Hepes, and, except for fura-2 experiments, Lucifer yellow 1 mg/ml. Membrane currents were measured with the patch-clamp technique in the whole-cell recording configuration [O. P. Hamill, A. Marty, E. Neher, B. Sakmann, F. J. Sigworth, *ibid.* **391**, 85 (1981)]. Current signals were amplified with conventional electronics (EPC-7 amplifier, List Electronics, Darmstadt, Germany), filtered at 3 kHz, and sampled at 5 kHz by an interface connected to an AT-compatible computer system, which also served as a stimulus generator.
6. Individual Bergmann glial cells were patch-clamped with pipettes containing 200 μM fura-2 in the tip and normal pipette solution in the rest of the pipette. In the whole-cell recording configuration, cells including their processes were filled with fura-2 within 10 to 40 min. The dye was excited at 340 and 380 nm with epifluorescence equipment (Axioplan Zeiss, Ober-kochen, Germany), and the resulting fluorescence signals were recorded with an intensified charge-coupled device camera (Hamamatsu, Hamamatsu City, Japan). The Ca^{2+} transients are shown as the ratio of the fluorescence intensity measured during excitation at 340 nm (F_{340}) and the fluorescence intensity measured during excitation at 380 nm (F_{380}) [G. Grynkiewicz, M. Poenie, R. Y. Tsien, *J. Biol. Chem.* **260**, 3440 (1985)]. Subcellular changes in Ca^{2+} concentration could be analyzed by selecting sections from the digitized image signals, and the pixels in these sections were averaged and extrapolated to continuous traces.
7. During recording, cells were filled with Lucifer yellow by dialyzing the cytoplasm with the patch pipette solution. To avoid destruction of the cell as the pipette was pulled off after recording, we destroyed the seal with a large hyperpolarizing current injection. After recording, slices were fixed for 3 to 5 hours at room temperature in 4% paraformaldehyde and 0.25% glutaraldehyde in 0.1 M phosphate buffer (pH 7.2). Slices were then transferred to phosphate buffer. Lucifer yellow–filled cells were examined in a microscope equipped with the appropriate filter combination (band pass, 400 to 440 nm; mirror, 460 nm; long pass, 470 nm).
8. After electrophysiology, slices were stained for glial fibrillary acidic protein (GFAP) by indirect immunofluorescence. Incubation with antibodies to GFAP (5 μg/ml diluted in 0.5% Triton X-100 in phosphate buffer, clone G-A-5) [E. Debus, U. Weber, M. Osborne, *Differentiation* **25**, 193 (1983)] was carried out overnight. Staining was visualized with goat antibody to mouse immunoglobulin. Slices were mounted with buffered glycerol.
9. I. Findlay, *Pfluegers Arch.* **410**, 313 (1987).
10. M. Ito, *The Cerebellum and Neural Control* (Raven, New York, 1984).

11. Supported by the Bundesministerium für Forschung und Technologie, the Deutsche Forschungsgemeinschaft (Heisenberg-Stipendium to H.K.; SFB 317), and the Boehringer-Ingelheim-Fonds (to T.B.). We thank P. Jonas, A. Konnerth, B. Sakmann, and W. Walz for helpful discussion.

21 January 1992; accepted 10 April 1992

Calcium-Permeable AMPA-Kainate Receptors in Fusiform Cerebellar Glial Cells

N. Burnashev, A. Khodorova, P. Jonas, P. J. Helm, W. Wisden, H. Monyer, P. H. Seeburg, B. Sakmann*

Glutamate-operated ion channels (GluR channels) of the L-α-amino-3-hydroxy-5-methyl-4-isoxazolepropionic acid (AMPA)–kainate subtype are found in both neurons and glial cells of the central nervous system. These channels are assembled from the GluR-A, -B, -C, and -D subunits; channels containing a GluR-B subunit show an outwardly rectifying current-voltage relation and low calcium permeability, whereas channels lacking the GluR-B subunit are characterized by a doubly rectifying current-voltage relation and high calcium permeability. Most cell types in the central nervous system coexpress several subunits, including GluR-B. However, Bergmann glia in rat cerebellum do not express GluR-B subunit genes. In a subset of cultured cerebellar glial cells, likely derived from Bergmann glial cells, GluR channels exhibit doubly rectifying current-voltage relations and high calcium permeability, whereas GluR channels of cerebellar neurons have low calcium permeability. Thus, differential expression of the GluR-B subunit gene in neurons and glia is one mechanism by which functional properties of native GluR channels are regulated.

Glutamate-operated channels are present in both neurons and glial cells. In most types of neurons (*1*) and in astrocytes (*2*, *3*), the GluR channels of the AMPA-kainate type are characterized by outwardly rectifying steady-state current-voltage (*I-V*) relations and low divalent-cation permeability. In recombinant GluR channels, transiently expressed in a mammalian cell line or in amphibian oocytes, both properties have been traced to the presence of an arginine residue in the putative TM2 transmembrane segment of the GluR-B subunit. Recombinant GluR channels containing a GluR-B (GluR-2) subunit show an outwardly rectifying *I-V* relation and a low permeability ratio P_{Ca}/P_{Cs}, whereas channels lacking a GluR-B subunit are characterized by a doubly rectifying *I-V* relation and a high permeability ratio P_{Ca}/P_{Cs} (*4*). In accordance with the finding that native GluR channels in most neurons and glial cell types show outward rectification and

N. Burnashev, P. Jonas, P. J. Helm, B. Sakmann, Max-Planck-Institut für Medizinische Forschung, Abteilung Zellphysiologie, Jahnstrasse 29, 6900 Heidelberg, Germany.
A. Khodorova, All-Union Research Institute of Biotechnology, Naychny Proezd 8, 117 246 Moscow, Russia.
W. Wisden, H. Monyer, P. H. Seeburg, Center for Molecular Biology, University of Heidelberg, 6900 Heidelberg, Germany.

*To whom correspondence should be addressed.